Comparative Study of DC-Link Capacitor Size for Two and Three Phase Permanent Magnet Synchronous Machines

Original
Comparative Study of DC-Link Capacitor Size for Two and Three Phase Permanent Magnet Synchronous Machines / Troncoso C., M.F., Stella, F., Pescetto, P., Pellegrino, G.. - 3:(2024), pp. 644-649. (2024 International Symposium on Power Electronics, Electrical Drives, Automation and Motion (SPEEDAM)) [10.1109/speedam61530.2024.10609065].

Availability:
This version is available at: 11583/2993868 since: 2024-10-30T09:01:37Z

Publisher:
IEEE

Published
DOI:10.1109/speedam61530.2024.10609065

Comparative Study of DC-Link Capacitor Size for Two and Three Phase Permanent Magnet Synchronous Machines

Matias F. Troncoso C., Fausto Stella, *Member IEEE*, Paolo Pescetto, *Member IEEE*, Gianmario Pellegrino, *Fellow IEEE*
Energy department *"Galileo Ferraris",* Politecnico di Torino, Turin, Italy
matias.troncoso@polito.it, fausto.stella@polito.it, paolo.pescetto@polito.it, gianmario.pellegrino@polito.it

***Abstract*—Two-phase open winding electrical machines have been proposed in the literature for their benefits in terms of peak torque and low noise emission. For this type of open-winding motors, a 4-leg power converter is required, allowing a power increase of 15% at the cost of one additional converter leg. This paper focuses on the impact of the two-phase open winding solution on the size of the DC-link capacitors, which is not covered in the literature. With reference to a state-of-the-art concentrated-winding 12slot/10pole 3ph PMSM drive, the DC-link RMS current stress and voltage ripple are comparatively analysed for different operating conditions. The simulations show that, under the same mechanical power conditions, the DC-link capacitor in the two-phase machine experiences lower voltage stress and similar RMS current compared to its three-phase counterpart. This effect impacts the cost, volume, and weight of the DC-link capacitor, partially compensating for the additional inverter leg required by the two-phase solution.**

Keywords — two phase machine, DC-link capacitor sizing, capacitor RMS current, capacitor voltage ripple, four leg inverter.

I. INTRODUCTION

The automotive sector is currently one of the main innovation leaders in high performance motor drives [1][2]. Significant advancements were recently achieved in the modelling, design and control of high-performance motors and converters [3]-[6], targeting high power density, reliability, efficiency and competitive cost. In this scenario, fractional slots concentrated windings electrical machines are often preferred against the distributed winding counterparts, as they present high torque and power density thanks to the short end-windings, which reduce the total motor length, at the cost of a higher magnetomotive force (MMF) harmonics. Among the concentrated winding machines, the 12slot-10pole three-phase Surface Permanent Magnet (SPM) synchronous motor is one of the most popular solutions for high-performance traction drives.

The studied two-phase 20slot-10pole open winding machine presents short end-windings, comparable with the fractional slot motors, and a high winding factor compatible with a distributed winding, together with good NVH (Noise, Vibration, and Harshness) performance [7]. Although this typology has been proposed for automotive applications [8], the related literature remains scarce. One drawback of this solution with respect to a standard three-phase drive is the addition of a 4^{th} inverter leg. Nevertheless, such additional leg allows a power increase of 15% [9]. This work focuses on the impact of this topology on the sizing of the DC link capacitor, which is a crucial aspect never been explored in prior studies.

The DC-link is among the most critical components of a two-level voltage source converter [10]. Two main design criteria are normally considered [11]-[14]: it must 1) comply with the maximum RMS current stress determined by the application, which generates acceptable losses and temperature rise in the capacitor, and 2) limit the peak-to-peak voltage ripple to a defined maximum threshold, to avoid altering the ideal inverter operation.

This study comprehensively analyses the DC-link capacitor stress within the operating range of both a standard three-phase machine and the proposed two-phase drive. Starting from the voltages and currents at the machine terminals (computed via FEM simulation) the stresses (i.e. RMS current and voltage ripple) on the DC-link capacitor are computed via numerical analysis.

II. COMPARISON OF 12S/10P AND 20S/10P MACHINES

In this study, a standard 3-phase 12s/10p SPM machine is compared with a 20s/10p open-end winding 2-phase counterpart, designed for equal inverter voltage and current rating, maximum speed, active length and stator diameter. The two motor topologies are presented in Table I. A cross-section of both motors is presented in Fig. 1, while the corresponding inverters are reported in Fig. 2 and Fig. 3. The maximum torque and speed envelop for the two topologies under test are compared in Fig. 4. As can be seen, the 20s/10p machine outperforms in torque and power the 12s/10p 3ph, as it has a higher winding factor, and the open winding configuration allows to use a higher voltage per winding. Otherwise said in the case of a two-phase machine supplied by a four-leg inverter it is possible to apply the full DC-link voltage to the machine phase thus reflecting in higher output power.

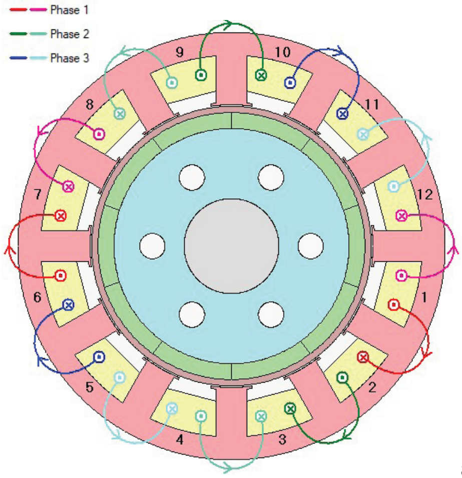

a)

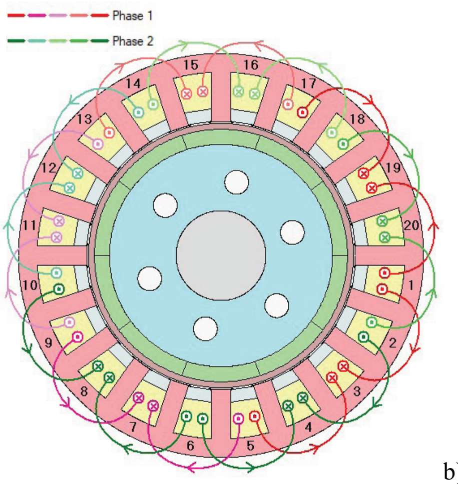

b)

Fig. 1. Cross section of the motors under comparison: a) 3ph 12 slot – 10 pole. b) 2ph 20 slot – 10 pole.

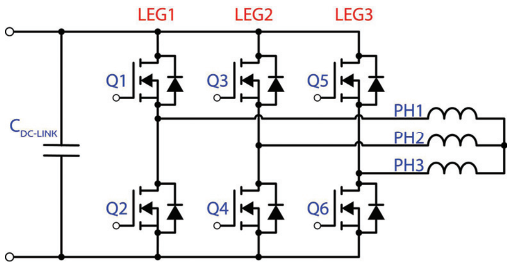

Fig. 2. 3-leg inverter for 3ph 12 slot – 10 pole machine.

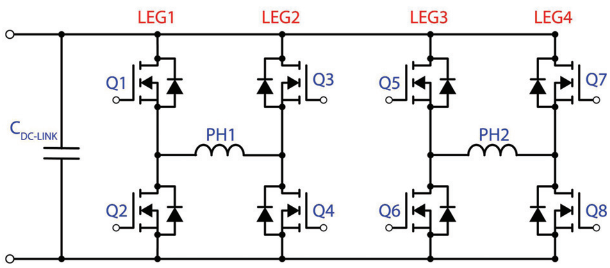

Fig. 3. 4-leg inverter for open winding 2ph 20 slot – 10 pole machine.

TABLE I. MOTOR TOPOLOGIES UNDER COMPARISON

Slot / Pole	12s/10p	20s/10p
Number of phases	3	2
Max. Phase Current	370Arms	370Arms
Max DC Voltage	700Vdc	700Vdc
Max. Speed	30krpm	30krpm
Winding Layer	Double Layer	Double Layer
Winding Topology	Fractional Slot	Integer Slot
Winding Throw	1	2 (overlapped)

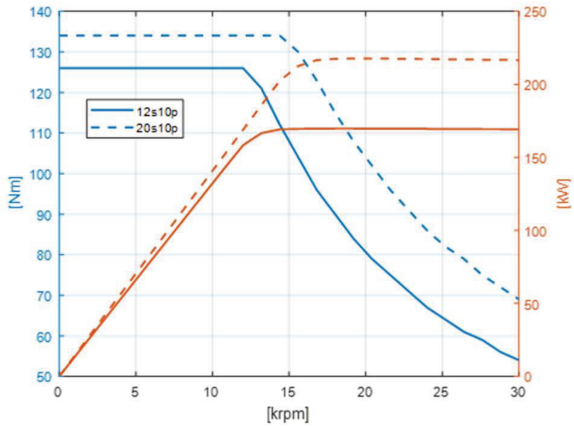

Fig. 4. Maximum performance curve for 2ph open winding 20s10p (dashed lines) versus 3ph 12s10p (solid lines)

III. DC-LINK STRESS FOR SINUSOIDAL LOAD CURRENT

The RMS current and voltage ripple stresses on the DC-link capacitor are numerically computed in the case of a three-leg and four-leg inverter supplying an ideal load absorbing a sinusoidal current. The results are reported in Fig. 5 and Fig. 6 for the three and four-leg inverters respectively.

In particular, the two subplots of Fig. 5 report the capacitor RMS current (left plot) and its charge ripple (right plot) for the three-leg inverter. The RMS current stress in the DC-link capacitor is plotted as a function of the modulation index and the power factor (e.g. the phase between load current and applied voltage) and normalized to the output phase current. For these simulations, a standard sinusoidal PWM technique with third harmonic voltage injection is adopted, i.e., the most common in 3-ph drives [11], [15]. This permits to reach a maximum modulation index of ≈1.15. Furthermore, it can be demonstrated that the choice of modulation technique does not have any impact on the RMS current in the capacitor [15]. The highest RMS current stress in the DC-link capacitor is found for a modulation index of ≈0.6 and cos(φ)=1, where the RMS current in the DC-link capacitor is 60% of the RMS phase current. In the right plot of Fig. 5, the normalized charge ripple $Q_{ripple,norm}$ in the DC-link capacitor is plotted against the modulation index and the power factor. The charge ripple is normalized to the switching frequency and the output RMS phase current:

$$Q_{ripple,norm} = Q_{ripple} \cdot \frac{f_{sw}}{I_{phase,RMS}} \tag{1}$$

Once the DC-link capacitor is selected, it is possible to compute the voltage ripple from the charge ripple.

$$\Delta v_{dc} = Q_{ripple,norm} \cdot \frac{I_{phase,RMS}}{f_{sw} \cdot C} \tag{2}$$

The highest normalized charge ripple, approximately 0.3, occurs at a modulation index of 1.15, again for a cos(φ)=1. It must be highlighted that, differently from the current stress, the charge and voltage ripples depend on the adopted modulation strategy [15]-[17].

The simulated capacitor stress for the four-leg inverter is reported in Fig. 6. Being an open winding motor, an eventual common-mode voltage injection would produce common mode current, with additional Joule loss without affecting the

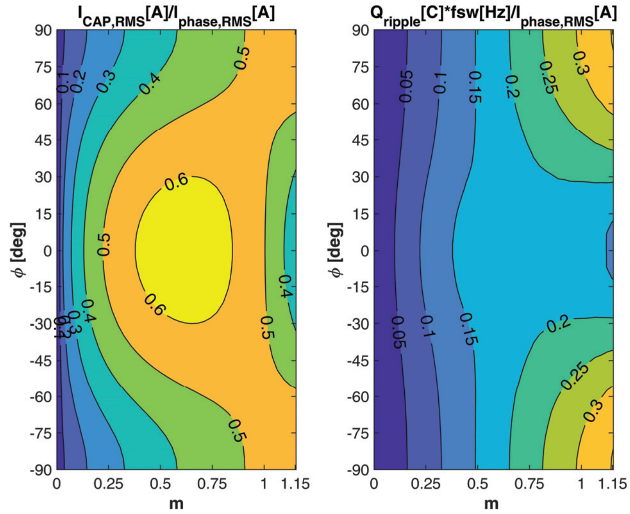

Fig. 5. **Three-leg inverter.** Left plot: RMS current in the DC-link capacitor normalized to the output phase current as a function of the modulation index m, and phase between output current and voltage ϕ. Right plot: ripple charge in the DC-link capacitors normalized to the switching frequency and phase current as a function of the modulation index m, and phase between the output current and voltage ϕ.

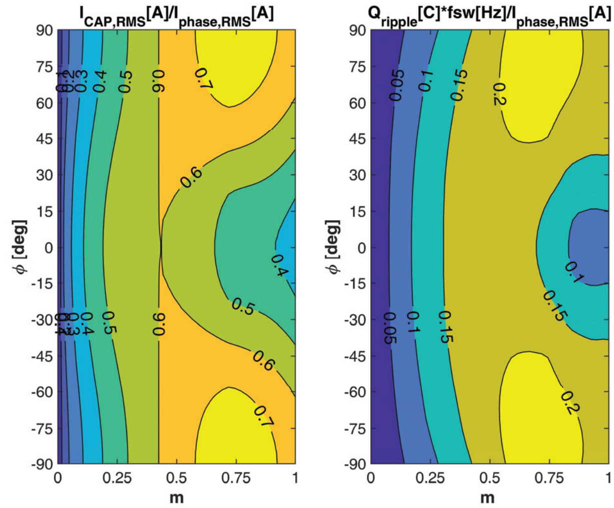

Fig. 6. **Four-leg inverter.** Left plot: RMS current in the DC-link capacitor normalized to the output phase current as a function of the modulation index m, and phase between output current and voltage ϕ. Right plot: ripple charge in the DC-link capacitors normalized to the switching frequency and phase current as a function of the modulation index m, and phase between the output current and voltage ϕ.

motor torque. For this reason, a sinusoidal modulation technique without common mode voltage injection is assumed while the leg load is set according to Fig. 3 (i.e. leg1 and leg2 have the same current but with opposite signs). The currents in the two phases are both sinusoidal but the phase shifted by 90 degrees, as expected in the 2-phase machine under test. Furthermore, leg1 and leg2 utilize the same triangular carrier, while the triangular carrier of leg3 and leg4 is interleaved with a phase shift of 90°. This configuration has been identified as optimal for minimizing stress on the DC-link capacitor, as confirmed through numerical analysis.

In the left plot of Fig. 6 the normalized RMS current stress in the DC-link capacitor is plotted, again as a function of the modulation index and the power factor. In this case, the highest current stress in the DC-link capacitor is for a modulation index of approximately 0.75 and cos(φ)=0, leading to an RMS current in the DC-link capacitor equal to 70% of the RMS phase current. Although this maximum capacitor current is considerably worse than the 3-phase case, it must be noted that the inverter of a motor drive does never realistically operate at such low values of power factor, with cos(φ) approaching to zero.

The right plot of Fig. 6 depicts the corresponding normalized charge ripple Q_{ripple} as a function of the modulation index and the power factor, for the four-leg inverter. The worst-case scenario is again in a non-realistic operating point for an electrical machine, with the highest normalized charge ripple, approximately 0.2, occurring at a modulation index of 0.75 and a cos(φ) value of 0.

IV. DC-Link Stress Under Real Operating Conditions

The analysis reported in Section III demonstrates that the most critical operating points, i.e. characterized by the maximum capacitor RMS current and voltage ripple, vary between the two converters. Therefore, the superiority of one configuration over the other depends on the required load cycle of the inverter.

For the application under test, i.e. a traction drive, for each point of the $T-n$ plane, the corresponding inverter voltage and current can be computed. A grid of points within the operating limits of the two machines, reported in Fig. 4, are simulated through Finite Element Analysis (FEA), obtaining the voltage waveform for each operating point. Based on the simulated voltage and current waveforms, the DC bus capacitor RMS current is evaluated, together with the expected charge ripple.

The following key assumptions are made:

- The current ripple on the machine due to the PWM modulation is neglected, as this does not impact significantly on the total DC-link capacitor RMS current and charge ripple as shown in [15].
- The DC-link capacitor exclusively contributes to the current resulting from PWM modulation, with the external DC source, i.e., a battery, providing the remaining current components, including DC and low-frequency AC components.

The RMS current in the DC-link capacitors as a function of speed and shaft torque for the two machines is shown in Fig. 7a) for the three-phase machine and in Fig. 7b) for the two-phase machine. The red line represents the maximum torque envelope, including the flux weakening region, so the data above the curve are of no use as the machine will never be able to operate in that region.

For the three-phase machine (Fig. 7a), the highest DC-link capacitor RMS current, reaching 203 A, occurs when the machine operates at a speed of 8800 rpm while providing a torque of 125 Nm. While for the two-phase machine (Fig. 7b)), the highest DC-link capacitor RMS current, reaching 245 A, occurs when the machine operates at a speed of 10600 rpm while providing a torque of 134 Nm. Although the capacitor RMS current is slightly higher for the two-phase machine, it is important to note that the machine is concurrently generating more mechanical power. If the RMS

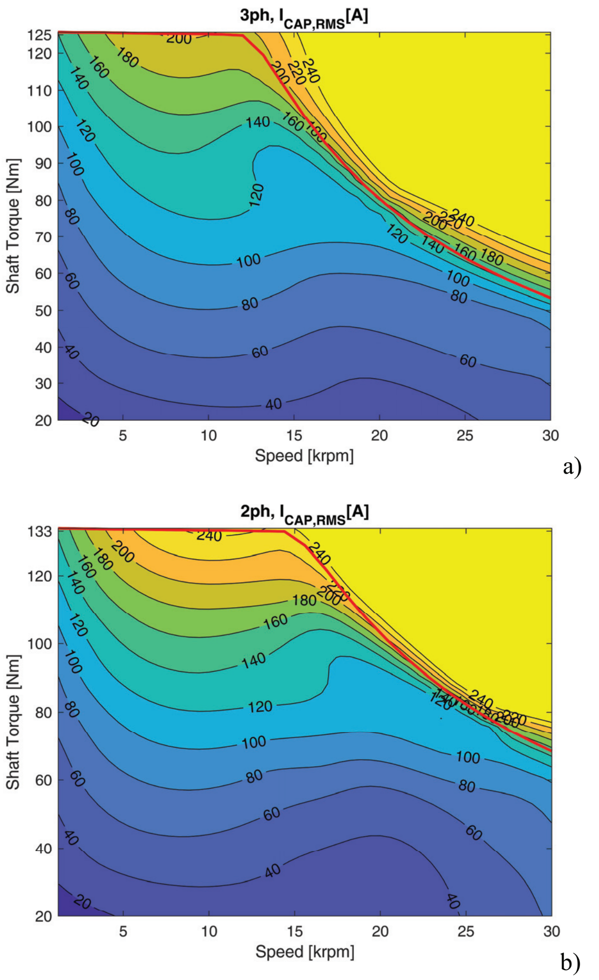

Fig. 7. DC link capacitor RMS current as a function of the speed and shaft torque. Red line represents the flux weakening curve limit, data on the right of the curve is not significant. a) three-phase machine b) two-phase machine.

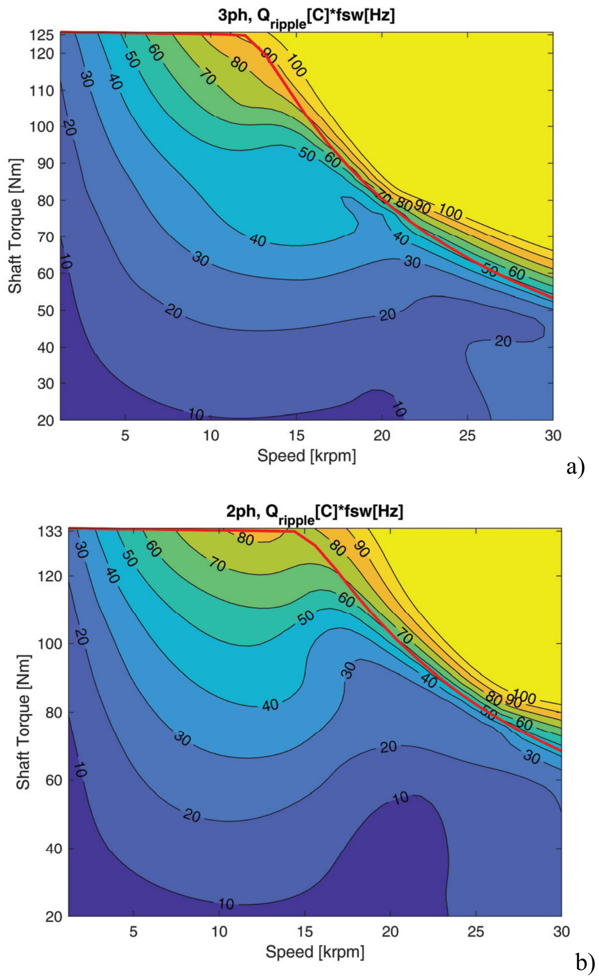

Fig. 8. DC link capacitor charge ripple as a function of the speed and shaft torque. Red line represents the flux weakening curve limit, data on the right of the curve is not significant. a) three-phase machine b) two-phase machine.

capacitor current is normalized to the peak mechanical power of the two machines, the values obtained are 0.0013 A/W for the three-phase machine and 0.0012 A/W for the two-phase machine. Consequently, it can be concluded that the current stress on the capacitor is comparable for both machines, with the two-phase machine demonstrating slightly better performance when the current is normalized to power.

The normalized charge ripple in the DC-link capacitors as a function of speed and shaft torque for the two machines is shown in Fig. 8a) for the three-phase machine and in 8b) for the two-phase machine. The absolute value of the charge ripple in the capacitor can be computed by dividing the normalized charge ripple by the switching frequency.

The maximum normalized charge ripple for the three-phase machine is 93 C·Hz, occurring at a torque of 126 Nm and a speed of 11770 rpm. In contrast, the two-phase machine exhibits its highest normalized charge ripple of 83 C·Hz when operating at a torque of 134 Nm and a speed of 12300 rpm. Remarkably, despite the higher power, the two-phase machine outperforms the three-phase machine in terms of charge ripple, indicating lower voltage ripple under the assumption of an equivalent DC-link capacitor value.

As said one of the main assumptions behind the proposed analysis is that the DC-link capacitor exclusively supplies the current resulting from PWM modulation, with the remaining current sourced from the battery. However, it may be interesting to analyse the current that the battery must provide to the converter. An ideal scenario involves a constant DC current, as it minimizes losses in the battery. Both converters draw a constant DC current when required to deliver perfectly sinusoidal currents and voltages, as outlined in Section III. However, in practical scenarios where these converters operate with real machines, the presence of subharmonics becomes inevitable, resulting in a non-constant current absorbed from the battery. In Fig. 9 and Fig. 10 the voltages and the currents obtained from the FEM simulation are shown together with the current absorbed from the battery for the three-phase and two-phase machines.

Fig. 9 shows the currents and the voltages on the three-phase machine when the machine is rotating at 14400 rpm and is delivering a torque of 111.2 Nm. The FEM simulator calculates the phase voltages that the inverter must apply to the machine to achieve sinusoidal phase currents. In a real-case scenario, the current control of the inverter would adjust the voltage applied to the machine to maintain sinusoidal currents. In this specific case, the phase voltages exhibit sinusoidal characteristics with just a negligible presence of subharmonics. This results in an almost constant current absorbed from the battery.

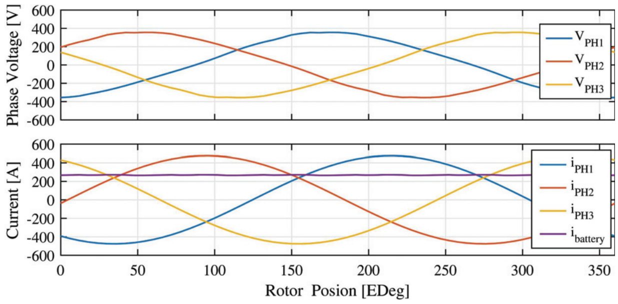

Fig. 9. **Three-phase machine** operating at 14400 rpm and 111.2 Nm with the 700 V DC-link. Top plot: phase voltages computed via FEM simulation. Bottom plot: phase and battery currents.

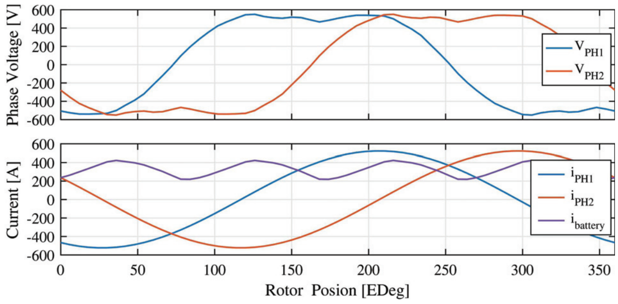

Fig. 10. **Two-phase machine** operating at 14400 rpm and 133 Nm with the 700 V DC-link computed via FEM simulation. Top plot: phase voltages. Bottom plot: phase and battery currents.

Fig. 10 reports the currents and voltages of the two-phase machine rotating at 14400 rpm and delivering a torque of 133 Nm. In this case, the phase voltages necessary to sustain a sinusoidal current in the machine are significantly distorted and the presence of subharmonics is visible. In addition, torque ripple is higher in the two-phase machine as presented in [1]. This is reflected in a non-constant current absorbed from the battery, with an AC component with a frequency that is four times the fundamental frequency of the phase current which reaches a peak-to-peak value of 180 A.

The peak-to-peak battery current ripple as a function of the speed and the shaft torque for the two machines is shown in Fig. 11a) for the three-phase machine and in Fig. 11b) for the two-phase machine. For the three-phase machine (Fig. 11a)), the highest battery current ripple is ≈20 A while for the two-phase machine is ≈180 A. This latter value can be considered critical especially if compared with the average current absorbed from the batter which is around 300 A. This AC component would result in additional losses and aging in the battery. This represents a major disadvantage of the machine taken as an example; however, the machine design can be improved by reviewing the electromagnetic design to lower the voltage harmonics and by introducing torque modulation strategies to reduce the torque ripple.

Furthermore, in a real case scenario when the machine is operating at high speed the frequency of the AC battery component becomes significant. For example, at 30000 rpm, the frequency of the AC current component in case of two-phase machine is 10 kHz, and part of this current will reasonably flow in DC-link capacitor. Therefore, the precise computation of the current sharing between the battery and the capacitor requires to know the total DC-link capacitance and the impedance of the connecting cable and any potential EMI filter between the battery and the DC-link capacitor.

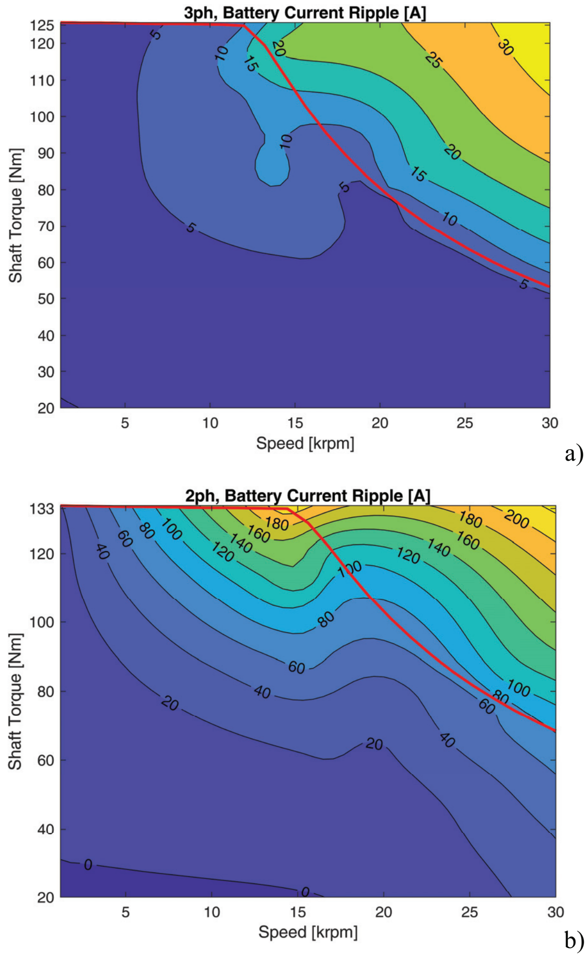

Fig. 11. Current ripple (peak to peak value) going to the battery as a function of the speed and shaft torque. The red line represents the flux weakening curve limit, data on the right of the curve is not significant. a) three-phase machine b) two-phase machine.

V. Conclusions

In this study, the DC-link capacitor RMS current stress was meticulously compared between a two-phase open-winding 20s10p machine, as proposed in [7], and a standard fractional slot three-phase 12s10p machine, utilizing Finite Element Method (FEM) and numerical analysis techniques. The findings unequivocally demonstrate that for identical mechanical output, the RMS current experienced by the DC-link capacitor remains comparable for both machines. Furthermore, it was observed that the charge ripple is lower for the two-phase machine under real operating conditions, indicating potential benefits in terms of stability and efficiency. Furthermore, a lower charge ripple reflects in a lower voltage ripple if the same DC-link capacitor is considered, this, in turn, enables to shrink the EMI filter that is among the bulkiest components of the converter [18], [19],[20]. Thermal unbalance and proper exploitation of the converter power switches may always been considered in future analysis, being this also important for the overall sizing of the converter [21],[22],[23] [24].

Our analysis pointed out that the proposed two-phase machine is introducing a “low frequency” AC current component to the battery current. This phenomenon, often disregarded in conventional literature analyses, inevitably leads to additional AC losses and accelerates battery aging, representing a significant limitation for this type of electrical machine [25]. However, it is essential to acknowledge that these drawbacks must be carefully weighed against the inherent advantages of the two-phase solution, particularly its enhanced power density and superior performance in terms of Noise, Vibration, and Harshness (NVH).

In summary, while the two-phase open-winding electrical machines offer promising benefits in peak torque and noise reduction, their implementation necessitates a careful consideration of the trade-offs involved. Balancing the potential drawbacks, such as increased AC losses and battery aging, with the advantages in power density and NVH performance is crucial for maximizing the utility of these innovative machine designs in practical applications.

Future work will be dedicated to the partial redesign of the two-phase machine with the aim of lowering the low-frequency AC component.

ACKNOWLEDGEMENTS

This study was carried out within the MOST – Sustainable Mobility Center and received funding from the European Union Next-GenerationEU (Piano Nazionale Di Ripresa E Resilienza (PNRR) – Missione 4 Componente 2, Investimento 1.4 – D.D. 1033 17/06/2022, CN00000023). This manuscript reflects only the authors' views and opinions, neither the European Union nor the European Commission can be considered responsible for them.

REFERENCES

[1] P. Hertzke, N. Müller, S. Schenk, and T. Wu, "The global electricvehicle market is amped up and on the rise," McKinsey Center for Future Mobility, Apr. 2018.

[2] M. Martino et Al., "Advanced Functionally Integrated E-Axle for A-Segment Electric Vehicles," 2020 AEIT International Conference of Electrical and Electronic Technologies for Automotive (AEIT AUTOMOTIVE), Turin, Italy, 2020, pp. 1-6, doi: 10.23919/AEITAUTOMOTIVE50086.2020.9307382.

[3] A. Krings and C. Monissen, "Review and Trends in Electric Traction Motors for Battery Electric and Hybrid Vehicles," 2020 International Conference on Electrical Machines (ICEM), Gothenburg, Sweden, 2020, pp. 1807-1813, doi: 10.1109/ICEM49940.2020.9270946.

[4] P. Pescetto, S. Ferrari, G. Pellegrino, E. Carpaneto and A. Boglietti, "Winding Thermal Modeling and Parameters Identification for Multithree Phase Machines Based on Short-Time Transient Tests," in *IEEE Transactions on Industry Applications*, vol. 56, no. 3, pp. 2472-2480, May-June 2020, doi: 10.1109/TIA.2020.2969643.

[5] P. Pescetto and G. Pellegrino, "Sensorless standstill commissioning of synchronous reluctance machines with automatic tuning," 2017 IEEE International Electric Machines and Drives Conference (IEMDC), Miami, FL, USA, 2017, pp. 1-8, doi: 10.1109/IEMDC.2017.8002302.

[6] S. Chowdhury, E. Gurpinar, G. -J. Su, T. Raminosoa, T. A. Burress and B. Ozpineci, "Enabling Technologies for Compact Integrated Electric Drives for Automotive Traction Applications," 2019 IEEE Transportation Electrification Conference and Expo (ITEC), Detroit, MI, USA, 2019, pp. 1-8, doi: 10.1109/ITEC.2019.8790594.

[7] M. F. Troncoso C., F. Stella and G. Pellegrino, "A Novel Two-Phase Permanent Magnet Rotor Machine for Automotive Applications," 2023 IEEE Workshop on Electrical Machines Design, Control and Diagnosis (WEMDCD), Newcastle upon Tyne, United Kingdom, 2023, pp. 1-6, doi: 10.1109/WEMDCD55819.2023.10110899.

[8] T. Stoyanov and R. Spasov, "Analysis of Two-phase Permanent Magnet Synchronous Machines Used for Hybrid Vehicles," 2018 10th Electrical Engineering Faculty Conference (BulEF), Sozopol, Bulgaria, 2018, pp. 1-3, doi: 10.1109/BULEF.2018.8646932.

[9] F. Zürcher, T. Nussbaumer, W. Gruber, and J. W. Kolar, "Comparison of 2- and 3-phase bearingless slice concepts," Journal of System Design and Dynamics, vol. 3, no. 4, pp. 471-482, 2008.

[10] M. Ciappa, "Selected failure mechanisms of modern power modules," Microelectronics Reliability, vol. 42, no. 4, pp. 653–667, Apr. 2002, doi: 10.1016/S0026-2714(02)00042-2.

[11] D. Cittanti et al., "Analysis, Design and Experimental Assessment of a High Power Density Ceramic DC-Link Capacitor for a 800 V 550 kVA Electric Vehicle Drive Inverter," IEEE Transactions on Industry Applications, pp. 1–13, 2023, doi: 10.1109/TIA.2023.3307101.

[12] H. Wen, W. Xiao, X. Wen, and P. Armstrong, "Analysis and Evaluation of DC-Link Capacitors for High-Power-Density Electric Vehicle Drive Systems," IEEE Transactions on Vehicular Technology, vol. 61, no. 7, pp. 2950–2964, Sep. 2012.

[13] P. Pescetto, A. Sierra-Gonzalez, F. Alvarez-Gonzalez, H. Kapeller, E. Trancho and G. Pellegrino, "Active Control of Variable DC-Link for Maximum Efficiency of Traction Motor Drives," in IEEE Transactions on Industry Applications, vol. 59, no. 4, pp. 4120-4129, July-Aug. 2023, doi: 10.1109/TIA.2023.3267770.

[14] Yifei Shao, Yongjun Cheng, Wenjing Zheng, Haifeng Guo, Dawei Li, Wubin Kong, "A Method for Calculating Current Harmonics and RMS of DC-Link Capacitor Considering AC Output Current Harmonics", 2023 26th International Conference on Electrical Machines and Systems (ICEMS), pp.722-726, 2023.

[15] J. W. Kolar, T. M. Wolbank and M. Schrodl, "Analytical calculation of the RMS current stress on the DC link capacitor of voltage DC link PWM converter systems," 1999. Ninth International Conference on Electrical Machines and Drives (Conf. Publ. No. 468), Canterbury, UK, 1999, pp. 81-89, doi: 10.1049/cp:19990995.

[16] J. Kolar, H. Ertl, and F. C. Zach, "Calculation of the Passive and Active Component Stress of Three-Phase PWM Converter Systems with High Pulse Rate," in European Conference on Power Electronics and Applications, vol. 3, Oct. 1989, pp. 1303–1311

[17] A. M. Hava, R. J. Kerkman and T. A. Lipo, "A high-performance generalized discontinuous PWM algorithm," in IEEE Transactions on Industry Applications, vol. 34, no. 5, pp. 1059-1071, Sept.-Oct. 1998.

[18] G. L. Skibinski, R. J. Kerkman and D. Schlegel, "EMI emissions of modern PWM AC drives," in IEEE Industry Applications Magazine, vol. 5, no. 6, pp. 47-80, Nov.-Dec. 1999, doi: 10.1109/2943.798337.

[19] F. Stella, E. Vico, D. Cittanti, C. Liu, J. Shen and R. Bojoi, "Design and Testing of an Automotive Compliant 800V 550 kVA SiC Traction Inverter with Full-Ceramic DC-Link and EMI Filter," 2022 IEEE Energy Conversion Congress and Exposition (ECCE), Detroit, MI, USA, 2022, pp. 1-8, doi: 10.1109/ECCE50734.2022.9948096.

[20] M. Kumar and K. Jayaraman, "Design of a Modified Single-Stage and Multistage EMI Filter to Attenuate Common-Mode and Differential-Mode Noises in SiC Inverter," in IEEE Journal of Emerging and Selected Topics in Power Electronics, vol. 10, no. 4, pp. 4290-4302, Aug. 2022, doi: 10.1109/JESTPE.2021.3133374.

[21] F. Stella, G. Pellegrino, E. Armando and D. Daprà, "Advanced testing of SiC power MOSFET modules for electric motor drives," 2017 IEEE International Electric Machines and Drives Conference (IEMDC), Miami, FL, USA, 2017, pp. 1-8, doi: 10.1109/IEMDC.2017.8002314.

[22] P. Korta, L. V. Iyer, A. Kundu, N. C. Kar and C. Pickersgill, "Over Temperature Protection During Hill-hold and Low-Speed Conditions for Electric Vehicle Traction Inverter," 2022 25th International Conference on Electrical Machines and Systems (ICEMS), Chiang Mai, Thailand, 2022, pp. 1-6, doi: 10.1109/ICEMS56177.2022.9982928.

[23] C. H. van der Broeck and R. W. D. Doncker, "Active Thermal Management for Enhancing Peak-Current Capability of Three-Phase Inverters," in 2020 IEEE Energy Conversion Congress and Exposition (ECCE), Oct. 2020, pp. 3312–3319.

[24] F. Stella, G. Pellegrino, S. Rubino and E. Armando, "Mitigation of the Performance Derating in SiC Motor Drive Inverters Operating at Low Output Current Frequency," 2023 IEEE Energy Conversion Congress and Exposition (ECCE), Nashville, TN, USA, 2023, pp. 4918-4924, doi: 10.1109/ECCE53617.2023.10362432.

[25] M. J. Brand, M. H. Hofmann, S. S. Schuster, P. Keil and A. Jossen, "The Influence of Current Ripples on the Lifetime of Lithium-Ion Batteries," in IEEE Transactions on Vehicular Technology, vol. 67, no. 11, pp. 10438-10445, Nov. 2018, doi: 10.1109/TVT.2018.2